Journal of Magnetism and Magnetic Materials 641 (2026) 173859

Contents lists available at ScienceDirect

Journal of Magnetism and Magnetic Materials

journal homepage: www.elsevier.com/locate/jmmm

Research article

Coherent coupling between YBCO superconducting resonators and sub-micrometer-thick YIG films☆

Alberto Ghirri [a,*], Mattia Cavani [b], Claudio Bonizzoni [b,a], Marco Affronte [b,a]

[a] Istituto Nanoscienze - CNR, Centro S3, via G. Campi 213/A, Modena, 41125, Italy
[b] Dipartimento di Scienze Fisiche, Informatiche e Matematiche, Universita di Modena e Reggio Emilia, via G. Campi 213/A, Modena, 41125, Italy

ARTICLE INFO

Keywords:
YIG
YBCO
Magnons
Microwaves
Strong coupling
Hybrid systems
Superconducting resonators

ABSTRACT

In cavity magnonics, magnon–photon hybridization has been widely investigated for both fundamental studies and applications. Planar superconducting resonators operating at microwave frequencies have demonstrated the possibility to achieve high couplings with magnons by exploiting the confinement of the microwave field in a reduced volume. Here we report a study of the coupling of high-T_c YBCO superconducting waveguides with 104-nm-thick YIG magnetic films. We study the evolution of mode frequencies as a function of temperature and extract the coupling strength of hybrid magnon–photon modes. We show that the experimental results can be reproduced using a simple model in which the temperature dependence of the penetration depth accounts for the evolution of the polaritonic spectrum.

1. Introduction

Magnon–photon hybrids are obtained by coherently coupling collective excitations in mgnetically ordered spin systems, that is spin waves and their quantized counterpart, magnons, with microwave photon modes. These systems have proven to be fertile ground for both fundamental studies and applications [1]. In the former case, topics like quantum magnonics [2,3], nonlinear effects [4–6], ultrastrong coupling [7–9], non-Hermitian physics [10,11], Floquet engineering [12], magnonic frequency combs [13] have been recently investigated. Applications in magnonics and quantum technologies, either at room temperature or in the quantum regime at mK temperatures, are related - but not restricted - to computation, sensing, microwave-to-optical transduction, coherent coupling of remote physical systems, and emission of microwaves [1,14–17].

For these studies, magnetic materials such as electrically insulating Yttrium Iron Garnet (YIG) or conducting permalloy, which are characterized by high spin densities and low ferromagnetic resonance (FMR) damping rates, have found widespread attention [18]. The embedding of these materials into superconducting circuits has opened additional possibilities [19–22]. Microwave modes in planar superconducting resonators have been exploited to achieve strong [23–26] and ultrastrong [9,27–30] coupling with magnons, also using nanomagnets fabricated directly onto the resonator [25,26]. Furthermore, superconducting qubits were coupled to YIG spheres to detect single-magnon excitations [2,31].

High critical temperature (T_c) superconducting resonators, in particular $YBa_2Cu_3O_7$ (YBCO), show T_c up to about 90 K and resilience to applied magnetic field [32]. Strong and ultrastrong coupling with spin systems have been achieved, respectively, using paramagnetic ensembles [33–37] and few-μm-thick YIG films [9,30]. In the latter case, the evolution of polaritonic modes at temperature below T_c has shown a progressive frequency shift of the hybrid magnon–photon mode, which has been correlated with the penetration depth in the superconducting layer as an effect of the interplay between Meissner currents and spin waves [30].

The spectrum of spin-wave excitations in the YIG film, as well as the coupling to the resonator, depend on the thickness of the magnetic layer. Here we experimentally investigate the evolution of transmission spectra obtained by placing a 104-nm-thick YIG film both on a broadband coplanar waveguide (CPW) and a half-wavelength CPW resonator fabricated from a YBCO film. We first study the broadband spectrum of excitations acquired using the YBCO CPW at different temperatures. We then analyze the coupling between microwave and magnon modes using the CPW resonator. We finally discuss how the extracted physical quantities compare with those obtained with thicker YIG films, which have been previously reported in Refs. [9,30].

2. Experimental methods

The broadband waveguide and the resonator were fabricated from a YBCO film having thickness of 330 nm (±10%), which was deposited

☆ This article is part of a Special issue entitled: 'Trends in Magnetism' published in Journal of Magnetism and Magnetic Materials.

* Corresponding author.
E-mail address: alberto.ghirri@nano.cnr.it (A. Ghirri).

https://doi.org/10.1016/j.jmmm.2026.173859
Received 7 March 2025; Received in revised form 10 September 2025; Accepted 17 January 2026
Available online 17 January 2026

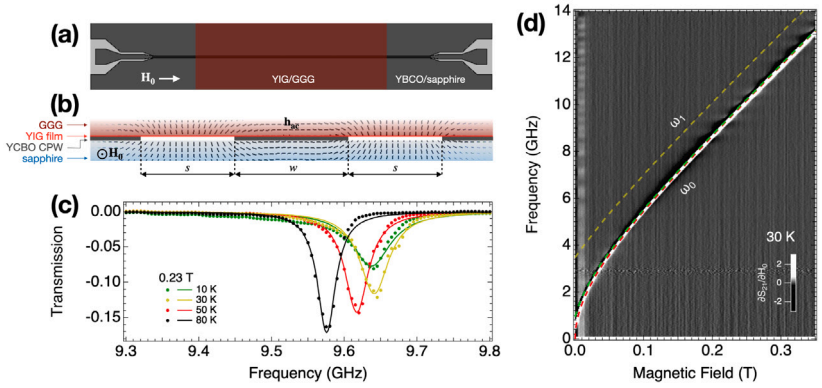

Fig. 1. Top view (a) and vertical section (b) of the CPW broadband line with the YIG film placed in top. Dashes in (b) show the distribution of the oscillating magnetic field $\mathbf{h}_{ac}$. (c) Evolution, at different temperatures, of the transmission spectra measured at $\mu_0 H_0 = 0.23$ T. The background S_{21} spectrum obtained from off resonance data has been subtracted. Solid lines display the Lorentzian fit (Eq. (1)). (d) Spectral map acquired at $T = 30$ K showing the derivative of transmission with respect to the magnetic field. Green and yellow dashed lines show ω_0 and ω_1 as derived respectively from Eqs. (2) and (4). The red dashed line show ω_{FMR}.

by reactive co-evaporation (RCE) [38] on a 3″-wide, 0.43-mm-thick, r-cut sapphire substrate with a 20-nm-thick CeO_2 buffer layer (Ceraco GmbH, M-type). The characteristic porous surface of the YBCO film shows enhanced flux pinning and critical current density higher than 2×10^6 A/cm^2 at 77 K. After deposition, the substrate was diced into $8 \times 5 \times 0.43$ mm^3 blocks, which were patterned using optical lithography and dry etching by Ar plasma in a Reactive Ion Etching (RIE) chamber. The central conductor of the CPW line has characteristic width w = 17 μm and separation s = 14 μm between the central conductor and the lateral ground planes (Fig. 1(a,b)). The broadband CPW supports transmission up to 14 GHz; the half-wavelength resonator has the same geometry except for two 140-μm-wide input and output capacitive gaps that interrupt the central conductor to define a central strip having length of 6 mm [9,30].

The YIG film that was grown by liquid phase epitaxy with thickness of 104 nm on a 0.5-mm-thick Gadolinium Gallium Garnet (GGG) substrate with (111) orientation (Matesy GmbH) [39]. The reported FMR linewidth is less than 2 Oe at room temperature.

The YIG/GGG film was cut in a $\approx 4 \times 2$ mm^2 sample and placed on the superconducting CPW. The film was gently pushed in contact with the YBCO surface by a plastic screw from the GGG side. The device was cooled down in a cryogenic setup equipped with a superconducting solenoid that generates the magnetic field (H_0), which is applied parallel to the central conductor of the CPW and to the YIG film (Fig. 1(a,b)). Transmission (S_{21}) measurements were carried out using a Vector Network Analyzer by sweeping the frequency at stationary values of the magnetic field. The incident microwave power is ≈ -8 dBm at the CPW input port. Test experiments carried out in the same conditions using a bare GGG sample have not shown any detectable magnetic resonance lines. The derivatives of the transmission, $\partial S_{21}/\partial H_0$ and $\partial^2 S_{21}/\partial H_0^2$, were calculated numerically.

3. Broadband transmission spectroscopy

We first used the broadband superconducting waveguide to study the evolution of ferromagnetic resonance lines. Transmission spectra evidence the presence of a main resonance at the frequency ω_0 (Fig. 1(c,d)). As the temperature (T) decreases, ω_0 progressively shifts toward higher frequencies. This trend indicates a decrease in the fixed-frequency resonance field as the temperature decreases between 80 K and 30 K. We fit the absorption dip, obtained by subtracting the background from the transmission spectra, using a Lorentzian curve [40]

$$\bar{S}_{21} = \frac{a}{1 + \left(\frac{\omega - \omega_0}{\frac{1}{2}\Delta\omega}\right)^2}, \tag{1}$$

where ω is the frequency, a is the amplitude and $\Delta\omega$ is the full width at half maximum (Fig. 1(c)). We note that $\omega_0/2\pi$ varies between 9.58 GHz at 80 K to 9.64 GHz at 10 K. The Lorentzian fits are in reasonable agreement with the measured resonance lines in Fig. 1(c), allowing us to obtain an estimation for $\Delta\omega/2\pi$, which increases from 30 MHz at 80 K to 64 MHz at 10 K.

When the YIG and YBCO layers are in good contact, an additional faint line can be observed at low temperature, whose frequency $\omega_1/2\pi$, is approximately 1.2 GHz above $\omega_0/2\pi$ (Fig. 1(d)). Fig. 2 shows the transmission maps taken at temperatures between 80 and 10 K, plotted as second derivative $\partial^2 S_{21}/\partial H_0^2$ to evidence ω_0 and ω_1. We note that spectra taken above 50 K show the presence of ω_0 only, while ω_1 is visible at 30 K and below.

Considering the lateral profile of the broadband CPW and the Damon–Eshbach geometry in our experiment, we expect that the transmission line excites spin wave modes with wavenumber up to $k_y = 3 \times 10^5$ rad m^{-1} $\approx 2\pi/s$ [30,41]. According to the analytical model by Kalinikos ans Slavin (KS) [42], the frequency of the lowest mode can be calculated as [43]

$$\omega_0/2\pi = \mu_0\gamma\sqrt{H_0(H_0 + M_s) + (M_s)^2 P_{00}(k_y d)\left(1 - P_{00}(k_y d)\right)}, \tag{2}$$

where γ = 28.02 GHz/T is the electron gyromagnetic ratio, $\mu_0 = 4\pi \times 10^{-7}$ H/m is the vacuum permeability and $P_{00} = 1 + [(1 - \exp(-k_y d))/k_y d]$. We note that, being d = 104 nm and $k_y d$ = 0.03, Eq. (2) results very close to $\omega_{FMR} = \mu_0\gamma\sqrt{H_0(H_0 + M_s)}$ (Fig. 1(d)). The temperature dependence of Eq. (2) derives from the saturation magnetization of YIG, M_s, which approximately follows [30,44,45]

$$M_s = M_0(1 - uT^{3/2} - vT^{5/2}), \tag{3}$$

being $u = 23 \times 10^{-6}$ K$^{-3/2}$ and $v = 1.08 \times 10^{-7}$ K$^{-5/2}$ [45]. Using $\mu_0 M_0$ = 0.28 T, we can reproduce the magnetic field dependence of ω_0 in the entire temperature range (Figs. 1(c,d) and 2).

Higher spin wave resonances beyond ω_0 are described in the KS model as Perpendicular Standing Spin Wave (PSSW) modes [42]. The frequency of the first PSSW mode is given by [43] (see the Eq. (4) in Box I) where A is the exchange constant of the YIG film. The experimental spectra in Figs. 1 and 2 can be reproduced using A = 5.2 pJ/m at 30 K and A = 5.5 pJ/m at 10 K.

4. Coupling between magnetic film and resonator

The 104-nm-thick YIG film was subsequently placed on top of the superconducting resonator to test the coupling between magnon and photon modes. At low temperature, the bare YBCO/sapphire resonator shows the fundamental mode at $\omega_c/2\pi \approx 10$ GHz, which decreases to $\omega_c/2\pi \approx 9.7$ GHz in the presence of the YIG/GGG sample.

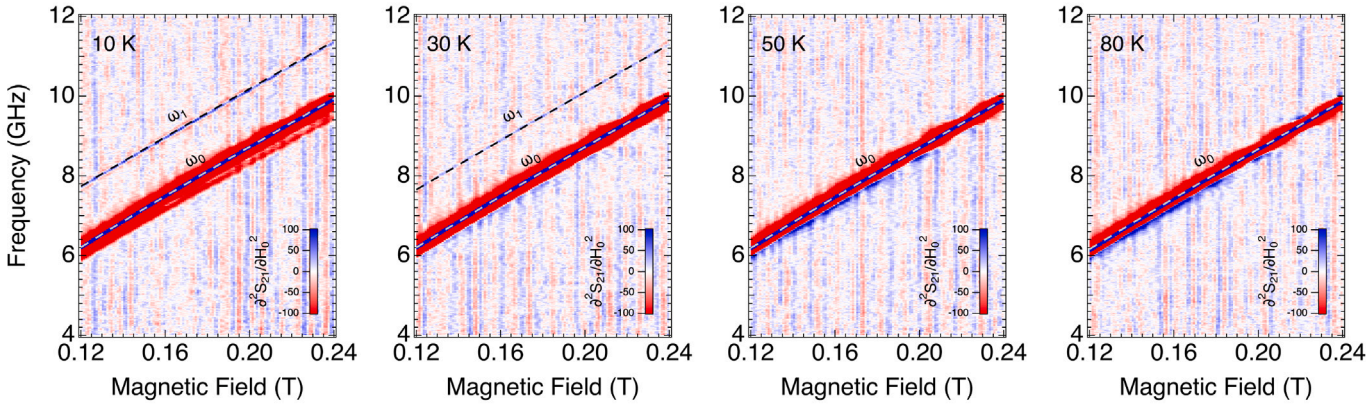

Fig. 2. Evolution of the spectral maps measured at different temperatures using the broadband CPW. The color scale shows the second derivative of transmission with respect to the magnetic field. Dashed lines display the curves calculated with Eqs. (2) and (4), as indicated.

$$\omega_1/2\pi = \gamma\mu_0\sqrt{\left[H_0 + \frac{2A}{M_s}\left(k_y^2 + \left(\frac{\pi}{d}\right)^2\right)\right]\left[H_0 + \frac{2A}{M_s}\left(k_y^2 + \left(\frac{\pi}{d}\right)^2\right) + M_s + H_0\left(\frac{Ms/H_0}{\pi/d}\right)^2 k_y^2\right]}, \tag{4}$$

Box I.

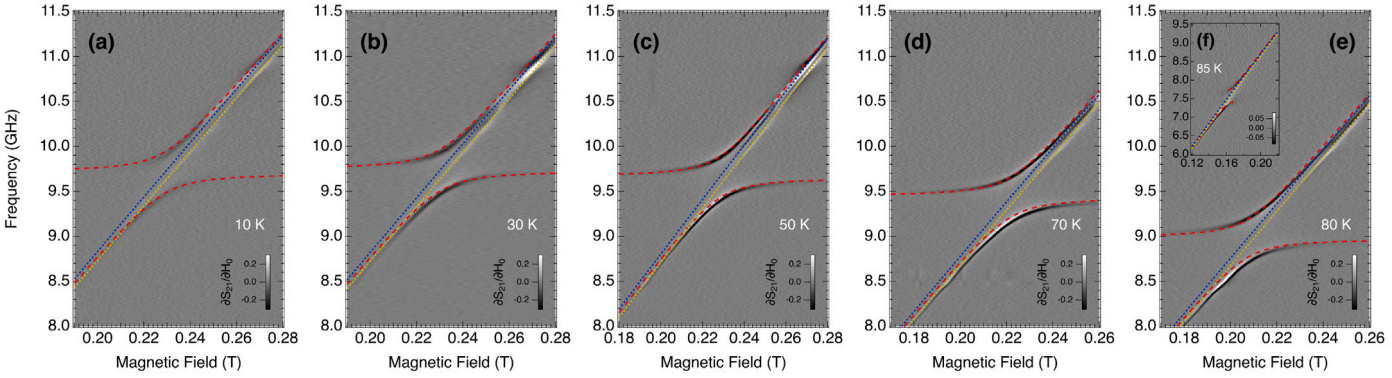

Fig. 3. Evolution of the transmission ($\partial S_{21}/\partial H_0$) spectra acquired as a function of temperature using the CPW resonator. The calculated polaritonic modes $\Omega_\pm$ are represented by red dashed lines; yellow and blue dashed lines show ω_0 and ω_b, respectively. The temperature value at which the map was taken is reported on each panel, from 10 K (a) to 85 K (f).

Magnon–photon hybridization is shown by the formation of polariton branches in transmission spectra displayed for a series of temperatures in Fig. 3. Below 50 K (panels (a–c)), the splitting of approximately 460 MHz corresponds to the collective coupling $g/2\pi \approx 230$ MHz. As the temperature increases, we observe the progressive lowering of the resonator frequency and the decrease in polariton splitting (panels (d–f)). The anticrossing disappears above T_c.

In order to extract meaningful parameters from the experimental spectra and compare them with previous results, we follow the analysis reported in [30]. The upper (Ω_+) and lower (Ω_-) polaritons can be described as the effect of the coupling between the resonator and a single magnetic mode (ω_b). Their evolution follows [9]

$$\Omega_\pm = \frac{1}{\sqrt{2}}\sqrt{\omega_c^2 + \omega_b^2 \pm \sqrt{\left(\omega_c^2 - \omega_b^2\right)^2 + 16\omega_c\omega_b g^2}}\,, \tag{5}$$

where ω_b is correlated to both magnetic field and temperature assuming that

$$\omega_b = \omega_0 + \delta_{sc}, \tag{6}$$

where ω_0 is the frequency of the lowest YIG mode (Eq. (2)) and δ_{sc} a temperature-dependent change. The latter can be quantified by self-consistently including the spin-wave induced Meissner currents in the Landau–Lifshitz–Gilbert equation, to obtain [21]

$$\delta_{sc} \approx \gamma\mu_0 M_s k_y dr \frac{1 - e^{-\frac{2t}{\lambda_L}}}{(k_y\lambda_L + 1)^2 - (k_y\lambda_L - 1)^2 e^{-\frac{2t}{\lambda_L}}}, \tag{7}$$

where t is the thickness of the YBCO film and r is a dimensionless geometrical factor associated with the YIG thickness and spin-wave ellipticity. λ_L is the penetration depth of YBCO, which in the simplest two-fluid binomial approximation reads [46]

$$\lambda_L = \frac{\lambda_L(0)}{\sqrt{1 - \left(\frac{T}{T_c}\right)^p}}, \tag{8}$$

where T_c is the critical temperature, $\lambda_L(0)$, is the London penetration length in the zero temperature limit, and $p = 4/3$ for d-wave superconductors [46–48].

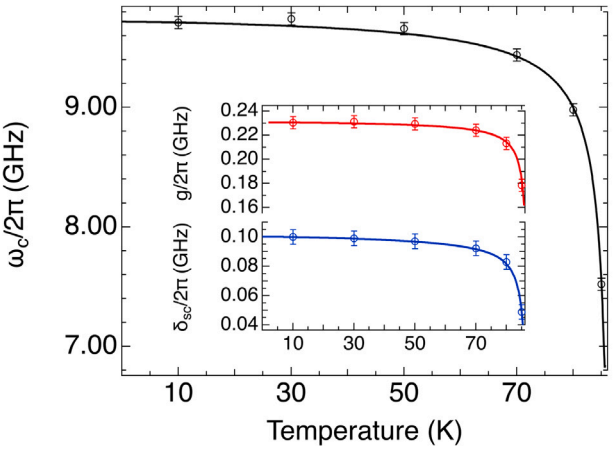

Fig. 4. Frequency of the resonator extracted from transmission maps acquired at different temperatures (circles). The solid line shows the fit with Eq. (9). Inset. Coupling strength and frequency shift derived using the fitted resonator frequency (circles) and Eq. (9) (solid lines). Error bars are estimated from the uncertainty of the fit parameters.

By means of Eq. (5) we have fitted the evolution of polaritons in Fig. 3. The frequency of the resonator, $\omega_c(T)$, is used at each temperature as a free parameter; ω_b has been calculated using Eq. (7), where $r = 0.45$ and the penetration depth has been derived from Eq. (8) with $T_c = 86.3$ K and $\lambda_L(0) = 104$ nm. The latter parameters are obtained from the fit of $\omega_c(T)$ (Fig. 4) using [48]

$$\omega_c \approx \omega_c(0)\sqrt{\frac{L[\lambda_L(T_0)]}{L[\lambda_L(T)]}}, \tag{9}$$

being $L[\lambda_L(T)]$ the temperature-dependent inductance and $\omega_c(0)/2\pi = 9.7$ GHz at $T_0 = 10$ K. Finally, the collective coupling $g = g_s\sqrt{2s_{\mathrm{Fe}}N_s}$, where $s_{\mathrm{Fe}} = 5/2$ is the single-ion spin of Fe^{3+}, is calculated assuming that the number of spins is $N_s = 1.49 \times 10^{13}$ in the entire temperature range. The temperature dependence of g derives, through $\omega_c(T)$, from the spin-photon coupling

$$g_s \approx \frac{\mu_0\omega_c}{4w}\sqrt{\frac{h}{Z_0}}, \tag{10}$$

where $Z_0 = 58\ \Omega$ is the nominal impedance of the CPW line [30] and $h = 6.626 \times 10^{-34}$ J s is the Planck constant.

Fig. 4 shows the temperature evolution of the parameters that describe the experimental data. From the fitted values of $\omega_c(T)$ and using the values of $\delta_{sc}(T)$ and $g(T)$ calculated using the parameters r and N_s, we can reproduce the evolution of the transmission spectra shown in Fig. 3 for temperatures between 10 and 85 K.

5. Discussion

It is worth comparing the results obtained here for the 104-nm-thick YIG film with those reported for thicker films [9,30]. The broadband spectra shown in Figs. 1 and 2 display two well-separated resonances at frequencies ω_0 and ω_1, in contrast with the larger number of closely spaced lines observed for a 5-μm-thick YIG film under similar experimental conditions [9,30]. The dependence of those two modes as a function of H_0 has been analyzed with Eqs. (2) and (4), using fitting parameters compatible with those previously reported [9,30,45,49]. In particular, Eq. (4) shows, in accordance with the trend observed in the experiments, an increase in the frequency ω_1 when the thickness of the YIG film decreases. The chosen fitting parameters account for the non-trivial evolution of the FMR line at low temperature, which has recently been attributed to the increase in magnetic anisotropy as a result of the interaction between the YIG film and the GGG substrate [39,50,51]. We note that the temperature evolution of the resonance position in Figs. 1(c) and 2, and the deviation from the Lorentzian line shape in the resonance spectra, are in line with other recently reported experiments [39,50].

The broadening of the lowest resonant peak and the diminishing of its amplitude at low temperature evidence the increase of losses (Fig. 1(c)). Despite the narrow FMR linewidths obtained at room temperature [52,53], low-temperature measurements on YIG/GGG films have shown FMR linewidths up to 30 MHz due to local defects and other effects induced by the GGG substrate [39,50,51]. Moreover, experiments with YIG films having conductive electrodes on top have shown the broadening of the FMR line [54–56]. Additional contributions to line broadening come from the superconductor. Inhomogeneities in the local magnetic field can be related to Meissner screening and non-perfect parallelism of the film surface with respect to the external magnetic field. Being our YBCO film a type-II superconductor with pinned vortices, in the mixed state we also expect the presence of inhomogeneous magnetic fields at the interface with the YIG film due to the presence of the Abrikosov lattice.

Additional fingerprints of the interplay between magnetic and superconducting layers can be found in the temperature-dependent properties of the YBCO CPWs. The amplitude of the microwave field decreases quasiexponentially as the height from the CPW increases [9] and, additionally, the penetration depth of YBCO drops to $\approx 100 - 150$ nm at low temperature [30]. The appearance of higher magnon modes in broadband measurements (Fig. 2) is likely due to the coupling between tightly confined microwaves and stray fields [41]. Furthermore, experiments with thick YIG films and YBCO resonators in the ultrastrong coupling regime evidenced the shift of the anticrossing position with respect to the unperturbed resonance line of the YIG film ($\delta_{sc}/2\pi$ up to 1.2 GHz) [30]. This behavior has been interpreted as an effect of electromagnetic proximity between the magnetic and superconducting layers [21,57].

In the present case, the 104-nm-thick YIG film gives rise to a much smaller shift ($\delta_{sc}/2\pi = 0.1$ GHz), which is justified by the smaller d in Eq. (7). However, the broadband spectra in Fig. 2 suggest that the line position at different temperatures can be reproduced using only the parameters of the YIG, without including the effect of the superconductor. We note that in Eq. (7) the geometric parameter r has been used as a free fitting parameter to adjust the absolute value of δ_{sc}; to better quantify its magnitude, a more systematic study that involves variations in the size and thickness of the YIG film would be required. Furthermore, we note that the estimated magnon and photon numbers are $N_m = N_p \approx 10^{10} \ll N_s$ [9]. The shifts in magnon frequency extracted from Fig. 3 are greater than those expected from the magnon Kerr effect in our experiment [58,59]. Considering the estimated mode volume of the resonator $V_m = N_s/\rho = 7 \times 10^{-14}$ m^3, being $\rho = 2.1 \times 10^{28}$ m^{-3} the spin density of the YIG, and the first-order anisotropy constant of the YIG film (K_{an}), we obtain the Kerr coefficient $K = \hbar\mu_0 K_{an}\gamma^2/(M_s^2 V_m) \approx 10^{-7}$ Hz. The Kerr effect results much lower than the collective spin-photon coupling. These numbers further confirm our analysis carried out in the linear regime with a low number of excitations.

We finally make a direct comparison between the coupling strength obtained and those reported in [9,30] using thicker YIG/GGG films and identical YBCO CPW resonator under similar experimental conditions. The maximum coupling strength derived from the spectra in Fig. 3 is 0.23 GHz while the coupling obtained with a 5-μm-thick YIG film having similar lateral size is around 1.1 GHz [30]. The ratio between thicknesses is 50 while the coupling strength achieved with the thicker film is only 5 times higher. By using wider 5-μm-thick films, the coupling strength increased to around 2 GHz, although no significant improvement was observed for thicknesses as high as 20 μm [9]. These results confirm that in our experiments a significant coupling with the CPW is achieved at distances below 1 μm above the YBCO surface.

6. Conclusions

In conclusion, we have studied the microwave response of non-conductive 104-nm-thick YIG films positioned on top of a YBCO superconducting layer. Transmission spectra were acquired at different temperatures either by using a broadband CPW or a CPW resonator. In the former case, experimental data have been essentially reproduced using well-consolidated models and physical quantities describing the spin-wave excitation spectrum of the YIG film. In the latter case, the coupling extracted from the splitting of magnon–photon polaritons amounts to 230 MHz. The changes in the polaritonic spectrum at different temperatures can be attributed to the effects of the penetration depth in the YBCO resonator. The comparison between results obtained with YIG films having different thicknesses suggests a non-trivial role of the system geometry and material parameters in determining the evolution of the transmission spectra.

CRediT authorship contribution statement

Alberto Ghirri: Writing – review & editing, Writing – original draft, Supervision, Methodology, Investigation, Funding acquisition, Formal analysis, Data curation. **Mattia Cavani:** Investigation. **Claudio Bonizzoni:** Writing – review & editing. **Marco Affronte:** Writing – review & editing, Supervision, Project administration, Funding acquisition.

Declaration of competing interest

The authors declare that they have no known competing financial interests or personal relationships that could have appeared to influence the work reported in this paper.

Acknowledgments

This work was partially supported by the project SMILE-SQUIP funded by the Italian NQSTI - National Quantum Science and Technology Institute code PE0000 0023 (M.A.) and by the U.S. Office of Naval Research Award No. N62909-23-1-2079 (M.A.). A.G. acknowledges financial support from PNRR MUR project ECS_00000033_ECOSISTER.

Data availability

Data will be made available on request.

References

[1] B. Zare Rameshti, S. Viola Kusminskiy, J.A. Haigh, K. Usami, D. Lachance-Quirion, Y. Nakamura, C.-M. Hu, H.X. Tang, G.E. Bauer, Y.M. Blanter, Cavity magnonics, Phys. Rep. 979 (2022) 1–61, URL https://www.sciencedirect.com/science/article/pii/S0370157322002460.

[2] D. Lachance-Quirion, Y. Tabuchi, S. Ishino, A. Noguchi, T. Ishikawa, R. Yamazaki, Y. Nakamura, Resolving quanta of collective spin excitations in a millimeter-sized ferromagnet, Sci. Adv. 3 (7) (2017) e1603150, http://dx.doi.org/10.1126/sciadv.1603150, URL https://www.science.org/doi/abs/10.1126/sciadv.1603150.

[3] H. Yuan, Y. Cao, A. Kamra, R.A. Duine, P. Yan, Quantum magnonics: When magnon spintronics meets quantum information science, Phys. Rep. 965 (2022) 1–74, http://dx.doi.org/10.1016/j.physrep.2022.03.002, URL https://www.sciencedirect.com/science/article/pii/S0370157322000977, quantum magnonics: When magnon spintronics meets quantum information science.

[4] Y.-P. Wang, G.-Q. Zhang, D. Zhang, T.-F. Li, C.-M. Hu, J.Q. You, Bistability of cavity magnon polaritons, Phys. Rev. Lett. 120 (2018) 057202, http://dx.doi.org/10.1103/PhysRevLett.120.057202, URL https://link.aps.org/doi/10.1103/PhysRevLett.120.057202.

[5] O. Lee, K. Yamamoto, M. Umeda, C.W. Zollitsch, M. Elyasi, T. Kikkawa, E. Saitoh, G.E.W. Bauer, H. Kurebayashi, Nonlinear magnon polaritons, Phys. Rev. Lett. 130 (2023) 046703, http://dx.doi.org/10.1103/PhysRevLett.130.046703, URL https://link.aps.org/doi/10.1103/PhysRevLett.130.046703.

[6] M.-X. Bi, H. Fan, X.-H. Yan, Y.-C. Lai, Folding state within a hysteresis loop: Hidden multistability in nonlinear physical systems, Phys. Rev. Lett. 132 (2024) 137201, http://dx.doi.org/10.1103/PhysRevLett.132.137201, URL https://link.aps.org/doi/10.1103/PhysRevLett.132.137201.

[7] J. Bourhill, N. Kostylev, M. Goryachev, D.L. Creedon, M.E. Tobar, Ultrahigh cooperativity interactions between magnons and resonant photons in a yig sphere, Phys. Rev. B 93 (2016) 144420, http://dx.doi.org/10.1103/PhysRevB.93.144420, URL https://link.aps.org/doi/10.1103/PhysRevB.93.144420.

[8] I.A. Golovchanskiy, N.N. Abramov, V.S. Stolyarov, A.A. Golubov, M.Y. Kupriyanov, V.V. Ryazanov, A.V. Ustinov, Approaching deep-strong on-chip photon-to-magnon coupling, Phys. Rev. Appl. 16 (2021) 034029, http://dx.doi.org/10.1103/PhysRevApplied.16.034029, URL https://link.aps.org/doi/10.1103/PhysRevApplied.16.034029.

[9] A. Ghirri, C. Bonizzoni, M. Maksutoglu, A. Mercurio, O. Di Stefano, S. Savasta, M. Affronte, Ultrastrong magnon-photon coupling achieved by magnetic films in contact with superconducting resonators, Phys. Rev. Appl. 20 (2023) 024039, http://dx.doi.org/10.1103/PhysRevApplied.20.024039, URL https://link.aps.org/doi/10.1103/PhysRevApplied.20.024039.

[10] D. Zhang, X.-Q. Luo, Y.-P. Wang, T.-F. Li, J.Q. You, Observation of the exceptional point in cavity magnon-polaritons, Nat. Commun. 8 (1) (2017) 1368.

[11] T. Yu, J. Zou, B. Zeng, J. Rao, K. Xia, Non-hermitian topological magnonics, Phys. Rep. 1062 (2024) 1–86, http://dx.doi.org/10.1016/j.physrep.2024.01.006, URL https://www.sciencedirect.com/science/article/pii/S0370157324000309, non-Hermitian topological magnonics.

[12] J. Xu, C. Zhong, X. Han, D. Jin, L. Jiang, X. Zhang, Floquet cavity electromagnonics, Phys. Rev. Lett. 125 (2020) 237201, http://dx.doi.org/10.1103/PhysRevLett.125.237201, URL https://link.aps.org/doi/10.1103/PhysRevLett.125.237201.

[13] J.W. Rao, B. Yao, C.Y. Wang, C. Zhang, T. Yu, W. Lu, Unveiling a pump-induced magnon mode via its strong interaction with walker modes, Phys. Rev. Lett. 130 (2023) 046705, http://dx.doi.org/10.1103/PhysRevLett.130.046705, URL https://link.aps.org/doi/10.1103/PhysRevLett.130.046705.

[14] D. Lachance-Quirion, Y. Tabuchi, A. Gloppe, K. Usami, Y. Nakamura, Hybrid quantum systems based on magnonics, Appl. Phys. Express 12 (2019).

[15] Y. Li, W. Zhang, V. Tyberkevych, W.-K. Kwok, A. Hoffmann, V. Novosad, Hybrid magnonics: Physics, circuits, and applications for coherent information processing, J. Appl. Phys. 128 (13) (2020) 130902, http://dx.doi.org/10.1063/5.0020277.

[16] P. Pirro, V.I. Vasyuchka, A.A. Serga, B. Hillebrands, Advances in coherent magnonics, Nat. Rev. Mater. 6 (12) (2021) 1114–1135, URL http://dx.doi.org/10.1038/s41578-021-00332-w.

[17] A.V. Chumak, P. Kabos, M. Wu, C. Abert, C. Adelmann, A.O. Adeyeye, J. Åkerman, F.G. Aliev, A. Anane, A. Awad, C.H. Back, A. Barman, G.E.W. Bauer, M. Becherer, E.N. Beginin, V.A.S.V. Bittencourt, Y.M. Blanter, P. Bortolotti, I. Boventer, D.A. Bozhko, S.A. Bunyaev, J.J. Carmiggelt, R.R. Cheenikundil, F. Ciubotaru, S. Cotofana, G. Csaba, O.V. Dobrovolskiy, C. Dubs, M. Elyasi, K.G. Fripp, H. Fulara, I.A. Golovchanskiy, C. Gonzalez-Ballestero, P. Graczyk, D. Grundler, P. Gruszecki, G. Gubbiotti, K. Guslienko, A. Haldar, S. Hamdioui, R. Hertel, B. Hillebrands, T. Hioki, A. Houshang, C.-M. Hu, H. Huebl, M. Huth, E. Iacocca, M.B. Jungfleisch, G.N. Kakazei, A. Khitun, R. Khymyn, T. Kikkawa, M. Kläui, O. Klein, J.W. Kłos, S. Knauer, S. Koraltan, M. Kostylev, M. Krawczyk, I.N. Krivorotov, V.V. Kruglyak, D. Lachance-Quirion, S. Ladak, R. Lebrun, Y. Li, M. Lindner, R. Macêdo, S. Mayr, G.A. Melkov, S. Mieszczak, Y. Nakamura, H.T. Nembach, A.A. Nikitin, S.A. Nikitov, V. Novosad, J.A. Otalora, Y. Otani, A. Papp, B. Pigeau, P. Pirro, W. Porod, F. Porrati, H. Qin, B. Rana, T. Reimann, F. Riente, O. Romero-Isart, A. Ross, A.V. Sadovnikov, A.R. Safin, E. Saitoh, G. Schmidt, H. Schultheiss, K. Schultheiss, A.A. Serga, S. Sharma, J.M. Shaw, D. Suess, O. Surzhenko, K. Szulc, T. Taniguchi, M. Urbanek, K. Usami, A.B. Ustinov, T. van der Sar, S. van Dijken, V.I. Vasyuchka, R. Verba, S.V. Kusminskiy, Q. Wang, M. Weides, M. Weiler, S. Wintz, S.P. Wolski, X. Zhang, Advances in magnetics roadmap on spin-wave computing, IEEE Trans. Magn. 58 (6) (2022) 1–72, http://dx.doi.org/10.1109/TMAG.2022.3149664.

[18] X. Han, H. Wu, T. Zhang, Magnonics: Materials, physics, and devices, Appl. Phys. Lett. 125 (2) (2024) 020501, http://dx.doi.org/10.1063/5.0216094.

[19] O.V. Dobrovolskiy, R. Sachser, T. Brächer, T. Böttcher, V.V. Kruglyak, R.V. Vovk, V.A. Shklovskij, M. Huth, B. Hillebrands, A.V. Chumak, Magnon–fluxon interaction in a ferromagnet/superconductor heterostructure, Nat. Phys. 15 (5) (2019) 477–482, http://dx.doi.org/10.1038/s41567-019-0428-5.

[20] I.A. Golovchanskiy, N.N. Abramov, V.S. Stolyarov, P.S. Dzhumaev, O.V. Emelyanova, A.A. Golubov, V.V. Ryazanov, A.V. Ustinov, Ferromagnet/superconductor hybrid magnonic metamaterials, Adv. Sci. 6 (16) (2019) 1900435, http://dx.doi.org/10.1002/advs.201900435, URL https://advanced.onlinelibrary.wiley.com/doi/abs/10.1002/advs.201900435.

[21] M. Borst, P.H. Vree, A. Lowther, A. Teepe, S. Kurdi, I. Bertelli, B.G. Simon, Y.M. Blanter, T. van der Sar, Observation and control of hybrid spin-wave–meissner-current transport modes, Sci. 382 (6669) (2023) 430–434, http://dx.doi.org/10.1126/science.adj7576, URL https://www.science.org/doi/abs/10.1126/science.adj7576.

[22] C.G.L. Bøttcher, N.R. Poniatowski, A. Grankin, M.E. Wesson, Z. Yan, U. Vool, V.M. Galitski, A. Yacoby, Circuit quantum electrodynamics detection of induced two-fold anisotropic pairing in a hybrid superconductor–ferromagnet bilayer, Nat. Phys. (2024) http://dx.doi.org/10.1038/s41567-024-02613-x.

[23] H. Huebl, C.W. Zollitsch, J. Lotze, F. Hocke, M. Greifenstein, A. Marx, R. Gross, S.T.B. Goennenwein, High cooperativity in coupled microwave resonator ferrimagnetic insulator hybrids, Phys. Rev. Lett. 111 (2013) 127003, http://dx.doi.org/10.1103/PhysRevLett.111.127003, URL https://link.aps.org/doi/10.1103/PhysRevLett.111.127003.

[24] R.G.E. Morris, A.F. van Loo, S. Kosen, A.D. Karenowska, Strong coupling of magnons in a yig sphere to photons in a planar superconducting resonator in the quantum limit, Sci. Rep. 7 (1) (2017) 11511, http://dx.doi.org/10.1038/s41598-017-11835-4.

[25] J.T. Hou, L. Liu, Strong coupling between microwave photons and nanomagnet magnons, Phys. Rev. Lett. 123 (2019) 107702, URL https://link.aps.org/doi/10.1103/PhysRevLett.123.107702.

[26] Y. Li, T. Polakovic, Y.-L. Wang, J. Xu, S. Lendinez, Z. Zhang, J. Ding, T. Khaire, H. Saglam, R. Divan, J. Pearson, W.-K. Kwok, Z. Xiao, V. Novosad, A. Hoffmann, W. Zhang, Strong coupling between magnons and microwave photons in on-chip ferromagnet-superconductor thin-film devices, Phys. Rev. Lett. 123 (2019) 107701, http://dx.doi.org/10.1103/PhysRevLett.123.107701, URL https://link.aps.org/doi/10.1103/PhysRevLett.123.107701.

[27] I.A. Golovchanskiy, N.N. Abramov, V.S. Stolyarov, V.V. Ryazanov, A.A. Golubov, A.V. Ustinov, Modified dispersion law for spin waves coupled to a superconductor, J. Appl. Phys. 124 (23) (2018) 233903, http://dx.doi.org/10.1063/1.5077086.

[28] I.A. Golovchanskiy, N.N. Abramov, V.S. Stolyarov, M. Weides, V.V. Ryazanov, A.A. Golubov, A.V. Ustinov, M.Y. Kupriyanov, Ultrastrong photon-to-magnon coupling in multilayered heterostructures involving superconducting coherence via ferromagnetic layers, Sci. Adv. 7 (25) (2021) eabe8638, http://dx.doi.org/10.1126/sciadv.abe8638, URL https://www.science.org/doi/abs/10.1126/sciadv.abe8638.

[29] I.A. Golovchanskiy, N.N. Abramov, O.V. Emelyanova, I.V. Shchetinin, V.V. Ryazanov, A.A. Golubov, V.S. Stolyarov, Magnetization dynamics in proximity-coupled superconductor-ferromagnet-superconductor multilayers. ii. thickness dependence of the superconducting torque, Phys. Rev. Appl. 19 (2023) 034025, http://dx.doi.org/10.1103/PhysRevApplied.19.034025, URL https://link.aps.org/doi/10.1103/PhysRevApplied.19.034025.

[30] A. Ghirri, C. Bonizzoni, M. Maksutoglu, M. Affronte, Interplay between magnetism and superconductivity in a hybrid magnon-photon bilayer system, Phys. Rev. Appl. 22 (2024) 034004, http://dx.doi.org/10.1103/PhysRevApplied.22.034004, URL https://link.aps.org/doi/10.1103/PhysRevApplied.22.034004.

[31] D. Xu, X.-K. Gu, H.-K. Li, Y.-C. Weng, Y.-P. Wang, J. Li, H. Wang, S.-Y. Zhu, J.Q. You, Quantum control of a single magnon in a macroscopic spin system, Phys. Rev. Lett. 130 (2023) 193603, http://dx.doi.org/10.1103/PhysRevLett.130.193603, URL https://link.aps.org/doi/10.1103/PhysRevLett.130.193603.

[32] A. Ghirri, C. Bonizzoni, D. Gerace, S. Sanna, A. Cassinese, M. Affronte, Yba2cu3o7 microwave resonators for strong collective coupling with spin ensembles, Appl. Phys. Lett. 106 (18) (2015) 184101, http://dx.doi.org/10.1063/1.4920930.

[33] C. Bonizzoni, A. Ghirri, M. Affronte, Coherent coupling of molecular spins with microwave photons in planar superconducting resonators, Adv. Phys.: X 3 (1) (2018) 1435305, http://dx.doi.org/10.1080/23746149.2018.1435305.

[34] C. Bonizzoni, A. Ghirri, F. Santanni, M. Atzori, L. Sorace, R. Sessoli, M. Affronte, Storage and retrieval of microwave pulses with molecular spin ensembles, Npj Quantum Inf. 6 (1) (2020) 68, http://dx.doi.org/10.1038/s41534-020-00296-9.

[35] C. Bonizzoni, M. Maksutoglu, A. Ghirri, J. van Tol, B. Rameev, M. Affronte, Coupling sub-nanoliter bdpa organic radical spin ensembles with ybco inverse anapole resonators, Appl. Magn. Reson. 54 (1) (2023) 143–164, http://dx.doi.org/10.1007/s00723-022-01505-8.

[36] Z. Velluire-Pellat, E. Maréchal, N. Moulonguet, G. Saïz, G.C. Ménard, S. Kozlov, F. Couëdo, P. Amari, C. Medous, J. Paris, R. Hostein, J. Lesueur, C. Feuillet-Palma, N. Bergeal, Hybrid quantum systems with high-$t_c$superconducting resonators, Sci. Rep. 13 (1) (2023) 14366, URL http://dx.doi.org/10.1038/s41598-023-41472-z.

[37] C. Bonizzoni, A. Ghirri, F. Santanni, M. Affronte, Quantum sensing of magnetic fields with molecular spins, Npj Quantum Inf. 10 (1) (2024) 41, http://dx.doi.org/10.1038/s41534-024-00838-5.

[38] H. Kinder, P. Berberich, W. Prusseit, S. Rieder-Zecha, R. Semerad, B. Utz, Ybco film deposition on very large areas up to 20x20 cm2, Phys. C: Supercond. 282–287 (1997) 107–110, http://dx.doi.org/10.1016/S0921-4534(97)00230-X, materials and Mechanisms of Superconductivity High Temperature Superconductors V. URL https://www.sciencedirect.com/science/article/pii/S092145349700230X.

[39] J.-Y. Kim, D.-G. Lee, D.-S. Um, J.W.A. Robinson, M.-J. Jin, Impact of interface paramagnetism and local defects on low-temperature magnetic properties of yig thin films on ggg, Phys. Rev. Mater. 9 (2025) 084409, http://dx.doi.org/10.1103/6sy6-tgs6, URL https://link.aps.org/doi/10.1103/6sy6-tgs6.

[40] C.P. Poole, H.A. Farach, Lineshapes in electron spin resonance, Bull. Magn. Reson. 1 (1979) 162–194, URL https://ismar.org/wp-content/uploads/2021/09/BMR_01_162-194_1979.pdf.

[41] I.S. Maksymov, M. Kostylev, Broadband stripline ferromagnetic resonance spectroscopy of ferromagnetic films, multilayers and nanostructures, Phys. E: Low-Dimensional Syst. Nanostructures 69 (2015) 253–293, http://dx.doi.org/10.1016/j.physe.2014.12.027, URL https://www.sciencedirect.com/science/article/pii/S1386947714004664.

[42] B.A. Kalinikos, A.N. Slavin, Theory of dipole-exchange spin wave spectrum for ferromagnetic films with mixed exchange boundary conditions, J. Phys. C: Solid State Phys. 19 (35) (1986) 7013, http://dx.doi.org/10.1088/0022-3719/19/35/014.

[43] S.O. Demokritov, A.N. Slavin, Spin Waves, Springer International Publishing, Cham, 2021, pp. 281–346, http://dx.doi.org/10.1007/978-3-030-63210-6_6.

[44] J. Solt, H. Irvin, Temperature dependence of YIG magnetization, J. Appl. Phys. 33 (3) (2004) 1189–1191, http://dx.doi.org/10.1063/1.1728651.

[45] H. Maier-Flaig, S. Klingler, C. Dubs, O. Surzhenko, R. Gross, M. Weiler, H. Huebl, S.T.B. Goennenwein, Temperature-dependent magnetic damping of yttrium iron garnet spheres, Phys. Rev. B 95 (2017) 214423, http://dx.doi.org/10.1103/PhysRevB.95.214423, URL https://link.aps.org/doi/10.1103/PhysRevB.95.214423.

[46] R. Prozorov, R.W. Giannetta, Magnetic penetration depth in unconventional superconductors, Supercond. Sci. Technol. 19 (8) (2006) R41, URL http://dx.doi.org/10.1088/0953-2048/19/8/R01.

[47] O. Vendik, I. Vendik, D. Kaparkov, Empirical model of the microwave properties of high-temperature superconductors, IEEE Trans. Microw. Theory Tech. 46 (5) (1998) 469–478, http://dx.doi.org/10.1109/22.668643.

[48] G. Ghigo, D. Botta, A. Chiodoni, R. Gerbaldo, L. Gozzelino, F. Laviano, B. Minetti, E. Mezzetti, D. Andreone, Microwave dissipation in ybco coplanar resonators with uniform and non-uniform columnar defect distribution, Supercond. Sci. Technol. 17 (8) (2004) 977, http://dx.doi.org/10.1088/0953-2048/17/8/004.

[49] A.M. Zyuzin, A.G. Bazhanov, Temperature dependence of the exchange interaction constant in iron garnet films, J. Exp. Theor. Phys. Lett. 63 (7) (1996) 555–559, http://dx.doi.org/10.1134/1.567056.

[50] R.O. Serha, A.A. Voronov, D. Schmoll, R. Verba, K.O. Levchenko, S. Koraltan, K. Davídková, B. Budinská, Q. Wang, O.V. Dobrovolskiy, M. Urbánek, M. Lindner, T. Reimann, C. Dubs, C. Gonzalez-Ballestero, C. Abert, D. Suess, D.A. Bozhko, S. Knauer, A.V. Chumak, Magnetic anisotropy and ggg substrate stray field in yig films down to millikelvin temperatures, Npj Spintron. 2 (1) (2024) 29, http://dx.doi.org/10.1038/s44306-024-00030-7.

[51] D. Schmoll, A.A. Voronov, R.O. Serha, D. Slobodianiuk, K.O. Levchenko, C. Abert, S. Knauer, D. Suess, R. Verba, A.V. Chumak, Wavenumber-dependent magnetic losses in yttrium iron garnet–gadolinium gallium garnet heterostructures at millikelvin temperatures, Phys. Rev. B 111 (2025) 134428, http://dx.doi.org/10.1103/PhysRevB.111.134428, URL https://link.aps.org/doi/10.1103/PhysRevB.111.134428.

[52] C. Dubs, O. Surzhenko, R. Linke, A. Danilewsky, U. Bruckner, J. Dellith, Submicrometer yttrium iron garnet lpe films with low ferromagnetic resonance losses, J. Phys. D: Appl. Phys. 50 (20) (2017) 204005, http://dx.doi.org/10.1088/1361-6463/aa6b1c.

[53] Y. Rao, D. Zhang, H. Zhang, L. Jin, Q. Yang, Z. Zhong, M. Li, C. Hong, B. Ma, Thickness dependence of magnetic properties in submicron yttrium iron garnet films, J. Phys. D: Appl. Phys. 51 (43) (2018) 435001, http://dx.doi.org/10.1088/1361-6463/aade43.

[54] S.M. Rezende, R.L. Rodriguez-Suarez, M.M. Soares, L.H. Vilela-Leqo, D. Ley Dominguez, A. Azevedo, Enhanced spin pumping damping in yttrium iron garnet/pt bilayers, Appl. Phys. Lett. 102 (1) (2013) 012402, http://dx.doi.org/10.1063/1.4773993.

[55] S.A. Bunyaev, R.O. Serha, H.Y. Musiienko-Shmarova, A.J. Kreil, P. Frey, D.A. Bozhko, V.I. Vasyuchka, R.V. Verba, M. Kostylev, B. Hillebrands, G.N. Kakazei, A.A. Serga, Spin-wave relaxation by eddy currents in $y_3fe_5o_{12}$/Pt bilayers and a way to suppress it, Phys. Rev. Appl. 14 (2020) 024094, http://dx.doi.org/10.1103/PhysRevApplied.14.024094, URL https://link.aps.org/doi/10.1103/PhysRevApplied.14.024094.

[56] D. Schmoll, R.O. Serha, J. Panda, A.A. Voronov, C. Dubs, M. Urbánek, A.V. Chumak, Elimination of substrate-induced fmr linewidth broadening in the epitaxial system yig-ggg by microstructuring, 2025, arXiv:2502.02978. URL https://arxiv.org/abs/2502.02978.

[57] Tao Yu, Xi-Han Zhou, Gerrit E.W. Bauer, I.V. Bobkova, Electromagnetic proximity effects at heterointerfaces, Phys. Rep. 1151 (2026) 1–94, http://dx.doi.org/10.1016/j.physrep.2025.10.002, https://www.sciencedirect.com/science/article/pii/S0370157325002777.

[58] Y.-P. Wang, G.-Q. Zhang, D. Zhang, X.-Q. Luo, W. Xiong, S.-P. Wang, T.-F. Li, C.-M. Hu, J.Q. You, Magnon kerr effect in a strongly coupled cavity-magnon system, Phys. Rev. B 94 (2016) 224410, http://dx.doi.org/10.1103/PhysRevB.94.224410, URL https://link.aps.org/doi/10.1103/PhysRevB.94.224410.

[59] G. Zhang, Y. Wang, J. You, Theory of the magnon kerr effect in cavity magnonics, Sci. China Phys. Mech. Astron. 62 (8) (2019) 987511.